A VARIATIONAL MODEL FOR DENOISING HIGH ANGULAR RESOLUTION DIFFUSION IMAGING

M. Tong[1], Y. Kim[2], L. Zhan[3], G. Sapiro[4], C. Lenglet[5], B.A. Mueller[6], P.M. Thompson[3], L.A. Vese[1]

[1]Dept. of Mathematics, University of California, Los Angeles
[2] Dept. of Mathematics, University of California, Irvine
[3] Laboratory of Neuroimaging, Dept. of Neurology, University of California, Los Angeles
[4]Dept. of Electrical and Computer Engineering, University of Minnesota
[5]Center for Magnetic Resonance Research, University of Minnesota
[6]Dept. of Psychiatry, University of Minnesota

ABSTRACT

The presence of noise in High Angular Resolution Diffusion Imaging (HARDI) data of the brain can limit the accuracy with which fiber pathways of the brain can be extracted. In this work, we present a variational model to denoise HARDI data corrupted by Rician noise. Numerical experiments are performed on three types of data: 2D synthetic data, 3D diffusion-weighted Magnetic Resonance Imaging (DW-MRI) data of a hardware phantom containing synthetic fibers, and 3D real HARDI brain data. Experiments show that our model is effective for denoising HARDI-type data while preserving important aspects of the fiber pathways such as fractional anisotropy and the orientation distribution functions.

1. INTRODUCTION

High angular resolution diffusion imaging (Tuch et al. [1, 2]) is a modality of magnetic resonance imaging (MRI) used in reconstructing the fiber directions in the brain. Water diffuses preferentially along the directions of fiber pathways, so knowing how water diffuses in the brain gives information regarding the orientation of fibers. The relationship between the MRI signal and water diffusion based on the Stejskal-Tanner equation [3], is $S(x,\theta,\phi) = S_0(x)\exp\left(-b\cdot d(x,\theta,\phi)\right)$, where $S(x,\theta,\phi)$ and $d(x,\theta,\phi)$ are the MRI signal and corresponding diffusion (spherical apparent diffusion coefficient, sADC) at x and in the direction $(\cos(\theta)\sin(\phi),\sin(\theta)\sin(\phi),\cos(\phi))$ on the sphere. $S_0(x)$ is the MRI signal at x when no diffusion gradient is applied, and b is a parameter used in collecting the data. Note that the true MRI signal $S(x,\theta,\phi)$ cannot be larger than the MRI signal without any diffusion gradient applied; i.e. $S(x,\theta,\phi) \le S_0(x)$ or $d(x,\theta,\phi) \ge 0$.

Acquired HARDI data is contaminated by noise, likely violating the constraints above, that can alter important characteristics of fiber pathways such as fractional anisotropy (FA) (see [4, 5, 6]), which measures the amount of anisotropy of water diffusion present in fibers. Thus, it is likely to be beneficial to denoise the HARDI data before attempting to extract fibers. Since MR diffusion weighted images are magnitudes of complex valued signals, and if the real and imaginary components of the signal are assumed to have Gaussian noise, the resulting magnitude image will have Rician distributed noise [7], given by: $Pr(S|u) = \frac{S}{\sigma^2}\exp(-\frac{S^2+u^2}{2\sigma^2})I_0(\frac{Su}{\sigma^2})$, where u is the underlying clean signal, S is the noisy signal, σ is the standard deviation of the noise, and I_0 is the zeroth-order modified Bessel function of the first kind. We refer to [8, 9] for more details about HARDI. Most relevant previous work can be found in [7, 10, 11, 12]. Our proposed model is different from [10] in that we incorporate the data acquisition model and from [11, 12] in that we impose a more accurate noise model, the Rician distributed one.

First, we present our variational denoising model and the numerical implementation of our algorithm. Following this, we perform numerical experiments on three sets of data. The first is 2D synthetic data; the second is 3D diffusion-weighted magnetic resonance imaging (DW-MRI) data of a hardware phantom containing synthetic fibers; the last is 3D real HARDI data of the brain. We provide numerical results to demonstrate the validity of our denoising model. We summarize our findings in the conclusions.

2. VARIATIONAL DENOISING MODEL

As in [11, 12], we consider the sADC, d, as unknown, and the recovered denoised HARDI signal u over Ω computed from d. We propose the variational model ($b = 1$):

$$\inf_{d:\Omega\mapsto\mathbb{R}^n}\Big\{F(d) = \int_\Omega |D(d)|dx$$

$$+\lambda\int_\Omega\sum_{i=1}^{n}\Big(-\log I_0\Big(\frac{S_iS_0e^{-P(d_i)}}{\sigma^2}\Big)+\frac{(S_0e^{-P(d_i)})^2}{2\sigma^2}\Big)dx\Big\},$$

where $\lambda > 0$ is a tuning parameter, S_i is the observed noisy HARDI signal measured in the spherical direction i, and d_i is the denoised unknown sADC in the same direction. We denote by $u_i = S_0 \exp(-P(d_i))$ the recovered denoised HARDI signal. P is a projection operator given by $P(z) = \begin{cases} z & \text{if } z \geq 0 \\ 0 & \text{if } z < 0 \end{cases}$, and $\int_\Omega |Dd| dx = \int_\Omega \sqrt{\sum_{i=1}^n |\nabla d_i|^2} dx$ is the vectorial total variation as a prior imposed on d. The first term acts as a regularization, and the second acts as a fidelity that incorporates the Rician distribution; up to a constant, it is equivalent to $-\log(P(S_i|S_0 \exp(-P(d_i))))$. The projection operator is introduced to satisfy the constraint $d_i \geq 0$.

To numerically implement the model described above, we consider the Euler-Lagrange equations in combination with the L^2 gradient descent method. The resulting evolution equations for $i = 1, ..., n$ are given by

$$\frac{\partial d_i}{\partial t} = \lambda P'(d_i)\Big(\frac{u_i^2}{\sigma^2} - \frac{I_1(\frac{S_i u_i}{\sigma^2})}{I_0(\frac{S_i u_i}{\sigma^2})}\frac{S_i u_i}{\sigma^2}\Big) + \nabla \cdot \Big(\frac{\nabla d_i}{\sqrt{\sum_{i=1}^n |\nabla d_i|^2}}\Big).$$

We discretize the above system of equations using finite differences and an iterative method. We define the initial guess

$$d_i(x) = \begin{cases} 0.005 & \text{if } S_i(x) > S_0(x) \\ -\log(S_i/S_0) & \text{if } S_i(x) \leq S_0(x), \end{cases} \quad (1)$$

to help satisfy the condition $d_i \geq 0$. Decreasing the constant 0.005 results in more violations of the constraint, while increasing it may lead to a less satisfactory numerical result.

For one of the data sets we consider, the standard deviation of the noise, σ, is unknown. To approximate σ, we use the identity $E(X^2) = A^2 + 2\sigma^2$ for a Rician distributed variable X; $E(X^2)$ is the expected value of X^2, and A is the true signal. Using portions of the data set (e.g. background) where we expect $A = 0$, we estimate $\sigma \approx \sqrt{E(X^2)/2}$.

3. NUMERICAL RESULTS

We perform numerical experiments on three sets of data to demonstrate the validity of the proposed denoising model.

First, we consider a 2D synthetic data set of size 8×8 with diffusion measured in $n = 94$ uniformly distributed directions at each spatial point. S_0 in this case is assumed to be a constant equal to 1. We create noisy data by adding Rician noise with standard deviation $\sigma = 0.01, 0.02, 0.04, 0.1$ and 0.2. The same σ used to create the noisy data is input as a known parameter in our denoising model (however, slightly different σ could also be used, or σ could be estimated from the data). We compute the diffusion orientation distribution function (ODF), which is a probability density function measuring the distribution of water diffusion in different directions on the sphere, for the ground truth, noisy, and denoised data (Fig. 1). ODFs are calculated using the tensor distribution function algorithm in [13]. Here, we use the Jensen-Shannon divergence (JSD) to measure the difference between the noisy/denoised ODF and the ODF of the ground truth. In all cases, the denoised data gives lower JSD values than those of the corresponding noisy data sets, indicating an increase in similarity to the ODF of the ground truth after denoising (Table 1). Also, root mean square error (RMSE) values between the denoised and ground truth MRI signals are lower than the RMSE values between noisy and ground truth MRI signals (Table 1). This suggests that we have a more accurate signal after denoising.

	JSD		RMSE	
σ	noisy	denoised	noisy	denoised
0.01	0.0044	0.0004	0.0100	0.0065
0.02	0.0102	0.0008	0.0201	0.0130
0.04	0.0441	0.0133	0.0396	0.0231
0.1	0.1578	0.0431	0.0986	0.0545
0.2	0.5423	0.1736	0.1950	0.0963

Table 1. Jensen-Shannon divergence (JSD) values between ODF of noisy/denoised and ODF of ground truth, and RMSE values between noisy/denoised signal and ground truth signal.

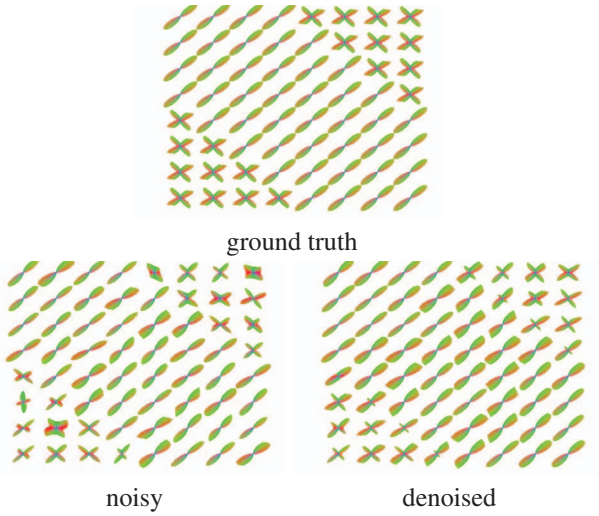


Fig. 1. Top: ODF of ground truth. Middle: ODF of noisy data generated with $\sigma = 0.2$. Bottom: ODF of denoised data.

Second, we consider DW-MRI data of a hardware phantom containing synthetic fibers created by Pullens et. al. [14]. The fibers ($\approx 10\mu$m circular diameter) consist of polyester yarns wound into bundles, which are then interdigitated on top of each other and secured with heat shrink tubes. A 7T scanner was used to collect the DW-MRI data from the phantom (data collection performed at the CMRR, University of Minnesota, on a Magnex Scientific MRI scanner driven by a Siemens console, with a head gradient insert capable of 80 mT/m in 200 ms. Parameter settings were: 66 slices with FOV=192 mm x 192 mm, 1.5x1.5x1.5 mm^3 voxels, TR/TE=5000/50ms, 128 DWI at b=1000 s/mm^2 and 15

	mean	standard deviation
noisy	0.2392	0.1503
denoised	0.2140	0.1292

Table 2. Mean and standard deviation values of FA for noisy and denoised phantom data.

b0 images). The dataset has an acquisition matrix of size $128 \times 128 \times 84$ and 100 uniformly distributed diffusion directions, but for computational purposes, we consider the 37th to 41st z-slices only and present T_2 and FA images for the 38th z-slice (Fig. 2). Given the way in which the fibers are constructed (i.e. from synthetic materials), the FA along the fiber should be approximately constant. In addition, ideally, the mean FA along a fiber should not drop after denoising, as a drop in FA can signify some loss in coherence, perhaps due to oversmoothing. As seen in Table 2, the mean FA drops slightly after denoising, but the standard deviation of the FA also decreases. After denoising, the FA correctly lies within a smaller range of values and is closer to being more constant along the fiber.

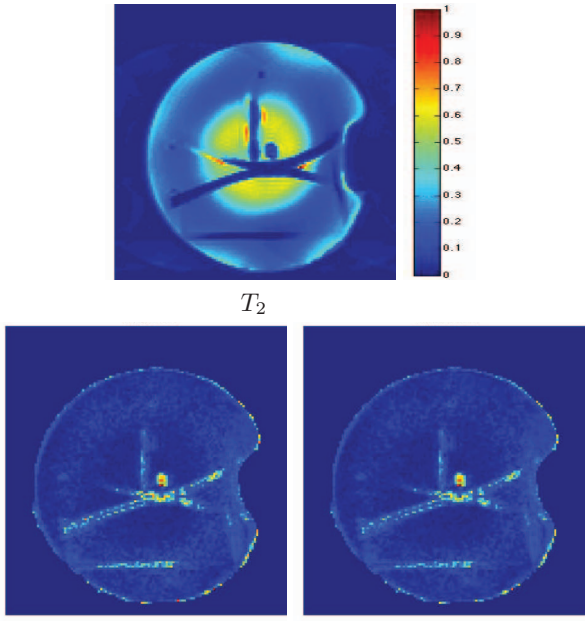


Fig. 2. Visualizations of 38th slice of phantom data. Top: T_2 visualization. Bottom left: FA visualization of noisy data. Bottom right: FA visualization of denoised data.

Lastly, numerical experiments were performed on real HARDI data of the brain. A healthy subject was scanned on a 4 Tesla Bruker Medspec MRI scanner with an optimized diffusion imaging sequence. Diffusion weighted imaging (DWI) parameters were: echo and repetition time, TE/TR 92.3/8250 ms, 55 x 2mm contiguous slices, field of view: FOV = 23 cm. 41 images were collected: 11 baseline (b0) images with no diffusion sensitization (i.e., T2-weighted images) and 30 diffusion-weighted images (b-value: 1159 s/mm^2) with gradient directions evenly distributed on the hemisphere. The reconstruction matrix was 128x128, yielding a 1.8x1.8 mm^2 in-plane resolution. This data was created by fitting actual HARDI data to a 6th order spherical harmonic expansion; the resulting data set is considered to be the "ground truth" (although this is not truly correct, it has artifacts and negative d values), and noisy data was generated by adding noise with $\sigma = 15$ to this "ground truth". The data set has volume $95 \times 128 \times 55$ and 30 uniformly distributed diffusion directions. We present in Fig. 3 the "ground truth", noisy, and denoised ODF's of the 30th z-slice. Fig. 4 shows the JSD between the noisy data and "ground truth" and between the denoised data and the "ground truth"; this figure shows that the similarity of the ODF to that of the "ground truth" is increased after denoising.

4. CONCLUSIONS

We presented a variational model to denoise HARDI-type data. We considered three types of data: 2D synthetic data with 94 directions, 3D DW-MRI data of a phantom consisting of synthetic fibers, and 3D real HARDI data of the brain. A comparison of the JSD values for the noisy versus denoised 2D synthetic data sets shows a higher similarity between the ODFs of the denoised result to that of the ground truth than between the ODF of the noisy data set to that of the ground truth. Furthermore, the denoised result for the phantom data gives more constant (and therefore more realistic) FA values along the fiber. Finally, ODF images for the real HARDI data show that the denoised ODF produces a better approximation to the ground truth ODF than the noisy ODF.

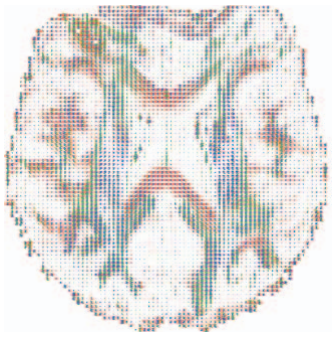
Acknowledgements: This work was funded by NIH (grants R01 EB008432, R01 EB007813, P41 RR008079, P41 EB015894, P30 NS057091, S10 RR026783), the W.M. Keck Foundation, and NSF grants CCF-0926127 and DMS-0714945.

5. REFERENCES

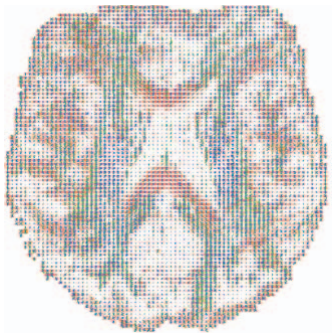
[1] D.S. Tuch, R.M. Weisskoff, J.W. Belliveau, and V.J. Wedeen, "High angular resolution diffusion imaging of the human brain," *Proc. 7th Annual Meeting of ISMRM*, p. 321, 1999.

[2] D.S. Tuch, T.G. Reese, M.R. Wiegell, N. Makris, J.W. Belliveau, and V.J. Wedeen, "High angular resolution diffusion imaging reveals intravoxel white matter fiber heterogeneity," *MRM*, pp. 577–582, 2002.

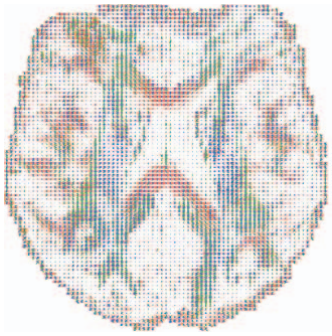
[3] E.O. Stejskal and J.E. Tanner, "Spin diffusion measurements: Spin echoes in the presence of a time-dependent field gradient," *JCP*, vol. 42, pp. 288–292, 1965.



ODF of clean data ("ground truth")

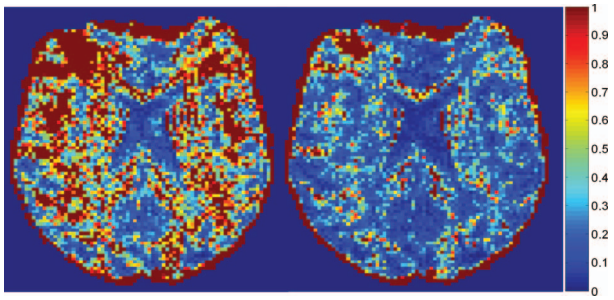


ODF of noisy data



ODF of denoised data

Fig. 3. ODF visualizations of 30th slice of real HARDI data. Top: "ground truth". Middle: noisy. Bottom: denoised. The color in this figure indicates the fiber direction: red for left-right, blue for superior-inferior, and green for anterior-posterior. Also, RMSE between noisy/denoised MRI signal and "ground truth" MRI signal: 14.9171 and 12.0868.



JSD of noisy data JSD of denoised data

Fig. 4. JSD between noisy and "ground truth" (mean = 0.5787, std. dev. = 0.3445) and between denoised and "ground truth" (mean = 0.3297, std. dev. = 0.3037) for the 30th slice of the real HARDI data. In the colorbar, we have values from 0 (blue) to 1 (red).

[4] C. Pierpaoli and P. Basser, "Toward a quantitative assessment of diffusion anisotropy," *MRM*, vol. 36, pp. 893–906, 1996.

[5] A.W. Anderson, "Theoretical analysis of the effects of noise on diffusion tensor imaging," *MRM*, vol. 46, pp. 1174–1188, 2001.

[6] S. Skare, T. Li, B. Nordell, and M. Ingvar, "Noise considerations in the determination of diffusion tensor anisotropy," *MRM*, vol. 18, pp. 659–669, 2000.

[7] S. Basu, T. Fletcher, and R. Whitaker, "Rician noise removal in diffusion tensor mri," in *LNCS 4190*. MICCAI, 2006, pp. 117–125.

[8] L.R. Frank, "Characterization of anisotropy in high angular resolution diffusion-weighted mri," *MRM*, vol. 47, pp. 1083–1099, 2002.

[9] C. Lenglet, JSW Campbell, M. Descoteaux, G. Haro, P. Savadjiev, D. Wassermann, A. Anwander, R. Deriche, G.B. Pike, G. Sapiro, K. Siddiqi, and P.M. Thompson, "Mathematical methods for diffusion mri processing," *NeuroImage, Special Issue on Mathematics in Brain Imaging*, 2008.

[10] T. McGraw, B. Vemuri, E. Özarslan, Y. Chen, and T. Mareci, "Variational denoising of diffusion weighted mri," *IPI*, vol. 3, pp. 625–648, 2009.

[11] Y. Kim, P.M. Thompson, and L. Vese, "Hardi data denoising using vectorial total variation and logarithmic barrier," *IPI, Special Issue in Medical Image Analysis*, vol. 4, pp. 273–310, 2010.

[12] Y. Kim, P.M. Thompson, A.W. Toga, L. Vese, and L. Zhan, "Hardi denoising : variational regularization of spherical apparent diffusion coefficients, sadc," *IPMI 2009, LNCS 5636*, pp. 515–527, 2009.

[13] A.D. Leow, S. Zhu, L. Zhan, K. McMahon, G.I. de Zubicaray, M. Meredith, M.J. Wright, A.W. Toga, and P.M. Thompson, "The tensor distribution function," *MRM*, vol. 61, pp. 205–214, January 2009.

[14] P. Pullens, A. Roebroeck, and R. Goebel, "Ground truth hardware phantoms for validation of diffusion-weighted mri applications," *JMRI*, vol. 32, pp. 482–488, April 2010.